Multi-fidelity Computational Fluid Dynamics of Aerosolized Viral Load Dispersion in the context of the COVID-19 Pandemic

Undergraduate Honors Thesis

By: Bella Barbera
Advisor: Dr. Yves Dubief
University of Vermont Mechanical Engineering

April 13th, 2021

Abstract

The impact of COVID-19, a world-wide pandemic, has left computational fluid dynamics center stage in developing risk management studies. Due to the airborne nature of COVID-19, the fluids community developed a role in modeling situations such as sneezing and coughing that serve as highly expiratory events due to the aerosolized virus. The recent increased ease of access to lower fidelity CFD software has created concern regarding if lower fidelity simulation softwares are able to effectively model and predict the dispersion of aerosols. Commonly, models are designed to deal with higher velocity flows, which is appropriate for investigations that have been aimed at high Reynolds number occurrences such as sneezing and coughing. Unfortunately, frequent actions such as relaxed breathing or nose-breathing are too commonly ignored due the misconception that they pose little risk of transmission. However, the resulting slow release of aerosols is generally undetectable, and therefore the debate arises as to if lower fidelity softwares designed for higher flows can accurately model situations such as these. Lower fidelity modeling options are often chosen due to their appealing simplicity and speed, however this generally comes at the price of oversimplifying the physics of the flow being modeled. This research investigates the limits of lower fidelity commercial software in modeling the dispersion of aerosols from nose breathing, and discusses the possible merits of multi-fidelity CFD as a tool to streamline decision making processes regarding community spread. The results from this study suggest value in continuing to pursue the use of multi-fidelity CFD, as it demonstrated the ability to reproduce similar qualitative results to the high-fidelity simulation. By continuing to fine-tune low fidelity modeling of the physics, this study provides evidence that a low fidelity code used in junction with a higher fidelity code, could certainly offer increases in computational efficiency.

Nomenclature

$\vec{A}$ = Surface Area Vector

a_1, a_2, a_3 = Constants to cover range of Reynolds Numbers

C_D = Drag Coefficient

C_U = Constant

C_1, C_2, C_3 = Constants

d_p = Particle Diameter

F_D = Drag Force

G_b = Generation of Turbulent Kinetic Energy due to buoyancy

G_k = Generation of Turbulent Kinetic Energy due to mean velocity gradients

k = Kinetic Energy

Re = Reynolds Number

S_k, S_ϵ = User Defined Source Sink Terms

S_ϕ = Source of ϕ per unit volume

t = Time

u = Phase Velocity

u_p = Particle Velocity

V = Volume

$\vec{v}$ = Velocity Vector

x = X-Distance

Y_M = Fluctuating dilatation in compressible turbulence to the overall dissipation rate

Δ_ϕ = Gradient of ϕ

ϵ = Specific Dissipation Rate

Γ_ϕ = Diffusion coefficient of ϕ

ϕ = Scalar Quantity being Transported

ρ = Density of the Fluid

ρ_p = Density of the Particle

σ_k = Turbulent Prandtl Numbers for k

σ_ϵ = Turbulent Prandtl Numbers for ϵ

μ = Molecular Viscosity of the Fluid

μ_t = Turbulent Eddy Viscosity

Contents

1 Objective and Introduction

1.1 Objective

Current research alludes to the idea that COVID-19 spreads predominantly through aerosols and droplets via the air, giving computational fluids modeling a great influence. This study aims to touch on an increasingly important concern regarding the accuracy of lower fidelity computational software (ANSYS Fluent) in modeling low Reynolds number flows. This is an extremely critical subject due to the lack of current research regarding lower Reynolds number flows with respect to aerosol dispersion. Lower fidelity codes often are able to perform swiftly due to an oversimplification of the physics of the flow, therefore it is crucial to understand where the limits lie with respect to low fidelity computational fluids modeling. The end goal of this study will be to gain an understanding regarding the accuracy in which ANSYS Fluent can perform in modeling aerosol dispersion at lower Reynolds numbers by comparing the results to a higher fidelity code YALES2.

1.2 Introduction

1.2.1 Background

Recently the world has been facing the unfamiliar and daunting challenge of the COVID-19 pandemic. The virus first emerged within China in late December of 2019, and since then

has expanded worldwide, provoking societal and economic shutdowns in order to combat the spread. Unaware of the lethality and infectious ability the virus possessed, health care centers around the world have been sent into distress, as hospitals reached maximum capacities. In addition to caring for those who have contracted the virus, a global effort has been put forth in preventing the spread via social distancing, face-coverings and more. Now just over a year from its emergence, a significant number of countries are still struggling to contain the spread of the virus enough despite social distancing efforts. In order to contain the exceedingly contagious virus, it is essential that the manner in which it spreads is well understood. The race to provide an accurate computational model that can display how the aerosols and droplets are spread through the air is an extremely important and weight bearing task. Many computational models fail to address key fluid flow phenomena that affects the behavior of how COVID-19 aerosols and droplets may be transported through the air. This includes but is not limited to, ghost turbulence (smaller voritces that can not properly be modeled by the general approaches taken by commercial fluid simulation software) as well as evaporation assumptions. This has been found to lead to error in investigations as high as 100%.[11] The incredible risk poised by these computational mishaps is the ability for this erroneous information to incorrectly inform society about the behavior of the virus. With proper investigation into the abilities and limits of low Reynolds number aerosol dispersion computational fluids modeling, greater trust can be invested into the simulations that are

guiding society in creating safety guidelines.

1.2.2 Transmission and Structure

Research regarding the virus has slowly progressed to suggest that contact contamination concerns, the direct transfer of the virus from a surface to the eyes, nose or mouth via touch, should not be the highest priority, as the virus appears to spread by aerosols and droplets. In other words, SARS-COVID-19 mainly spreads through the respiratory tract via human to human interactions due to contaminated droplets that contain the virus.[7] Spread can be exacerbated with sneezing, coughing, or speaking loudly which further accelerates the droplets away from the infected individual. Airborne transmission can be generally categorized into two infection mechanisms: 'close' infection due to large droplets and 'distant' infection due to small droplets that have the ability to remain airborne for long periods of time. Despite knowing this, the weight of importance regarding either 'close' or 'distant' infection for COVID-19 is still unknown. Smaller droplets that may be invisible to the naked eye, also bring up concern regarding quantifying the threat of asymptomatic or weakly symptomatic patients. Areas of importance involved in airborne transmission are droplet sedimentation and droplet evaporation.[8] These mechanisms are integral in characterizing the behavior of COVID-19 aerosols and droplets in the ambient environment after they are produced by an infected individual.

1.2.3 Behavior

In confined situations, it is remarkably important to be able to predict the evaporation and settling patterns in order to determine how long the droplet nuclei may remain airborne. Current research regarding airborne transmission suggests that most droplets expelled evaporate within a few seconds to form droplet nuclei. This process however may be slowed by vapor-rich, buoyant turbulent jet expiration. On the sub-micrometer scale (about 10 micrometer), these droplet nuclei may remain suspended in the air for hours. The half-life of these airborne virions is still under debate, but is currently estimated as 1.0-1.2 hours, which allows them to be considered a serious threat in contracting COVID-19, as the viral load necessary to contract the virus has not yet been confidently established.[8] The reason as to why air borne particles are not predicted to stay airborne for such extended periods of time, is due to to the fact that existing numerical studies commonly do not properly address small scales of turbulent mixing processes, which are critical with regards to droplet evaporation. Although these studies such as Euler-Lagrangian approaches and LES (Large Eddy Simulations) are appealing due to simplicity, they stand as a prime example of how the complexity of the flow physics must be validated by comparison with high fidelity simulations and experiments.[9]

Smaller droplets released often remain in the humid cloud of breath, which drastically slows the evaporation rates, which can be confirmed by referencing the corresponding shrink-

age rate when compared to the $d\hat{2}$ law which stands as the basis for Well's theory regarding isolated droplets. The behavior for smaller droplets is the opposite as they move more rapidly out of the vapor rich puff and actually evaporate quicker than predicted by the $d\hat{2}$ law due to the dominance of the convective effects as stated by.[9] In addition to the influence of the surrounding fluid, the effect of the local relative humidity surrounding droplets is a crucial factor of evaporation. For smaller droplets d = 10-100 micron, the relative surrounding humidity is higher than that of ambient air and decreases ad droplet diameter increases as they fall from the humid puff. However, beyond 100 micron the relative humidity is found to be higher than 10-100 micron, because the larger droplets evaporate greater volumes of vapor per time.[9] This effect although extremely local, due to the strong shear of the larger droplets, stands as a prime example as to why specific parameters must be calibrated correctly and compared with high fidelity codes. The simplicity of models mentioned earlier can fail to address the many physiochemical processes that affect droplet behavior. In this case the convective turbulent mixing and evaporation effects are the main focus, but others include and are not limited to, Brownian motion, gravity, electrostatic forces, thermal gradients, electromagnetic radiation, inertial forces, turbulent diffusion and convective effects.[12]

1.2.4 Computational Fluids: Methodology

Computational fluid dynamics (CFD) is a division of fluid mechanics that utilizes numerical analysis and data structures to evaluate and resolve problems involving fluid flows. The methodology takes advantage of computing power to perform numerous calculations regarding the free stream flow of the fluid as well as the flows interaction with defined boundary conditions. Reynolds-averaged Navier-Stokes equations are one of the most fundamental approaches in turbulence modeling. The version of the Navier-Stokes equations used in CFD are time-averaged equations of motion for fluid flow, with an additional term known as Reynolds stresses which is usually addressed by a selected turbulence model, many of which exist.[3] RANS can be addressed in two large general categories, the Boussineq hypothesis and the Reynolds stress model (RSM). The Boussinesq hypothesis uses an algebraic equation for the Reynolds stresses which addresses solving for turbulent viscosity and possibly turbulent kinetic energy and dissipation. The RSM actually solves the transport equations for the Reynolds stresses which may involve several equations and therefore a much greater CPU cost. RANS can be solved as a steady state simulation or transient. Steady-state computes the fully developed solution that does not change in time, using the mean values computed. Steady-state is a much lower CPU cost, but is a mean average for flow properties which can eliminate important aspects of the flow dynamics. Transient simulations can regain some of the lost dynamics due to steady state, as it computes the instantaneous values in each time

for each quantity, however this comes at a greater storage and computational cost.

One of the other most common models for simulating turbulence in CFD is a Large eddy simulation (LES). In LES, the smallest scales of the flow (about 20%) are removed and are remodeled using sub-grid scale models. Therefore the largest and "most important" scales of turbulence are able to be resolved while reducing computational time. Direct numerical simulation (DNS) is perhaps the most accurate and precise of all fluids modeling, as no turbulence model is used to solve the Navier-Stokes equations. This essentially indicates resolving the whole range of spatial and temporal scales of turbulence from the smallest dissipative scales. In order to accomplish this incredibly fine grids and extremely small time steps must be employed. The results are unparalleled, however this definite method cannot always be utilized due to its incredible computational cost.[4]

1.2.5 RANS Basic Structure

ANSYS Fluent is the lower fidelity software used in this experiment. The solver takes a Reynolds Averaging Navier Stokes or (RANS) approach in order to model the flow. Fluent uses a control-volume-based approach to adapt a general scalar transport equation to an algebraic equation that can be solved numerically. This control volume approach subsists of integrating the transport equation about each control volume, which yields a discrete equation that expresses the conservation law bases around a control-volume technique. The

following unsteady conservation equation for transport of a scalar quantity can be seen below:

$$\int_V \frac{\partial \rho\phi}{\partial t} dV + \oint \rho\phi\vec{v} \cdot d\vec{A} = \oint \Gamma_\phi \Delta\phi \cdot \vec{A} + \int_V S_\phi dV \tag{1}$$

Where ϕ is the scalar quantity being transported, ρ is density, $\vec{v}$ is a velocity vector, $\vec{A}$ is a surface area vector, Γ_ϕ is a diffusion coefficient of ϕ, Δ_ϕ is a gradient of ϕ, and S_ϕ is the source of ϕ per unit volume. It is this equation that is applied to each and every control volume in the computational domain. Commonly, RANS equations will be used to characterize turbulent flows due their ability to be used in junction with approximations based on knowledge of the properties of the flow turbulence to obtain time-averaged solutions to the Navier-Stokes equations. The equations used in RANS are time-averaged equations of motion for fluid flow, and originate from Reynolds Decomposition. Reynolds decomposition refers to separation of the flow variable (e.g. velocity u) into the mean (time-averaged) component ($\bar{u}$) and the fluctuating component (u'). When each instantaneous quantity is split into time averaged and fluctuating components and the resulting equations are time-averaged, the momentum equation can be obtained. Lastly, since integration in time removes the time dependence of the resultant terms, the time derivative is eliminated which leaves:

$$\frac{\partial \rho\bar{u}_i}{\partial_t} + \frac{\partial \rho\bar{u}_i\bar{u}_j}{\partial x_j} = \frac{\partial}{\partial x_j}\left[-\bar{p}\delta_{ij} + 2\mu\bar{S}_{ij} - \rho\overline{u_i'u_j'}\right] \tag{2}$$

$$\bar{S}_{ij} = \frac{1}{2}\left(\frac{\partial \bar{u}_i}{\partial x_j} + \frac{\partial \bar{u}_j}{\partial x_i}\right) \tag{3}$$

Where S_{ij} is the mean rate of strain tensor.[17] The change in mean momentum of a fluid element due to the unsteadiness and convection of the mean flow is balanced by a mean body force, the isotropic stress due to the mean pressure field, the viscous stresses and apparent stress due to the velocity field often known as the Reynolds stress. The Reynolds stress is the term that generally requires extensive modeling to close the RANS equations for solving and what gave rise to the creations of turbulence models.[17] With regards to the turbulent aspects of the flow, a $k-\epsilon$ turbulence model was employed which is applicable to free shear flows with relatively small pressure gradients as in this case. Seeing as the interest of the experiment lay in the aerosol behavior after being released from the cylinder, it was deemed appropriate to select a turbulence model that doesn't target accurate modeling of wall boundary layers. It is based off of model transport equations for the turbulent kinetic energy and specific dissipation rate. The turbulent kinetic energy k and the specific dissipation rate, ϵ are obtained from the transport equations below:

$$\frac{\partial}{\partial t}(\rho k) + \frac{\partial}{\partial x_i}(\rho k u_i) = \frac{\partial}{\partial x_j}[(\mu + \frac{\mu_t}{\sigma_k})\frac{\partial k}{\partial x_j}] + G_k + G_b - \rho\epsilon - Y_M + S_k \tag{4}$$

$$\frac{\partial}{\partial t}(\rho \epsilon) + \frac{\partial}{\partial x_i}(\rho u_i) = \frac{\partial}{\partial x_j}[(\mu + \frac{\mu_t}{\sigma_k})\frac{\partial \epsilon}{\partial x_j}] + C_{1\epsilon}\frac{\epsilon}{k}(G_k + C_{3\epsilon}G_b) - C_{2\epsilon}\rho\frac{\epsilon^2}{k} + S_\epsilon \tag{5}$$

Where G_k is the generation of turbulent kinetic energy due to mean velocity gradients and G_b is the generation of turbulence kinetic energy due to buoyancy. Y_M represents the contribution of the fluctuating dilatation in compressible turbulence to the overall dissipation rate. $C_{1\epsilon}$, $C_{2\epsilon}$ and $C_{3\epsilon}$ are constants. σ_k and σ_ϵ are the turbulent Prandtl numbers for k and ϵ respectively. S_k and S_ϵ are user defined source sink terms. The turbulent (eddy) viscosity μ_t is defined below where C_μ is a constant:[2]

$$\mu_t = \rho C_\mu \frac{k^2}{\epsilon} \tag{6}$$

1.2.6 Yales 2 Basic Structure

YALES2 is a high fidelity code that was developed by CORIA and the French Combustion and Fluid mechanics community. It is used by 250+ scientists and industry such as SAFRAN, ARIANE GROUP, SOLVAY, SIEMENS. YALES2 is a High Fidelity Large Eddy Simulation code, commonly known as (HFLES) which are commonly used in combustion and have the ability to simulate multiphase flows and transport all species (gas liquid). Essentially it works by simulating explicitly the larger eddies that contribute the most to the energy of turbulence, as well as modeling the contribution of smaller scales. To gain this level of accuracy, it comes at higher demands with respect to modeling the physics of the flow. This means abiding strictly by conservation of Energy requirements, for example a vortex lifetime

must not be cut short by numerical diffusion. The physics at play must also be properly respected with regards to geometries, thermodynamics of droplets, droplet size distribution, boundary conditions etc... Lastly, supercomputers must be used as efficiently as possible in order to be able to simulate all important scales of the flow.

2 Numerical Models and Methods

2.1 RANS

2.1.1 Physical Model

The physical model consisted only of a single cylinder, sized and oriented to represent the trajectory of a singular human nostril. The radius of the cylinder is 5mm as this is considered a average for a human.[13] The physical testing model was kept as simplistic as possible because the phenomena being investigated were able to be properly simulated with an elementary geometry. This was due to the fact that the subject of interest was the behavior of the aerosols once released from the orifice that represents a nostril, and not their behavior surrounding or within the cylinder orifice. The cylinder was placed at a height of 1.6 meters to simulate average nostril height and allow for proper downward migration. An enclosure of -0.75m to 2m along the X-Axis, -1.6m to 1m on the Y-Axis, and -1m to 1m in the Z-Axis is placed around the cylinder orifice to to replicate a closed room with no other

disturbances. The enclosure is large enough to avoid aerosol contact or any influence their behavior, but no larger as to cut down on computational time. The entire enclosure is 14.512 m^3. Figures 1 and 2 below show the physical layout of the model as described.

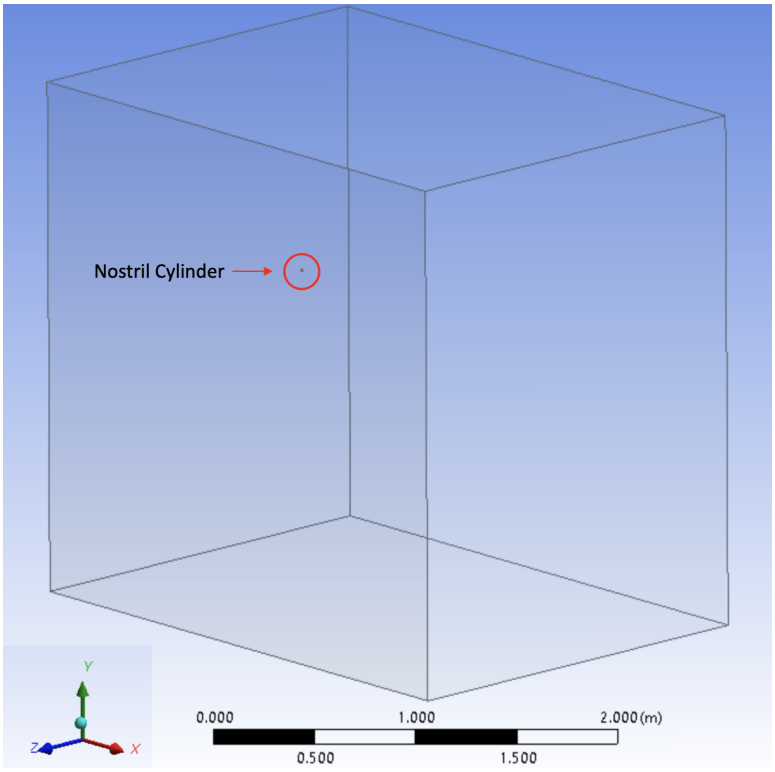

Figure 1: Physical Domain

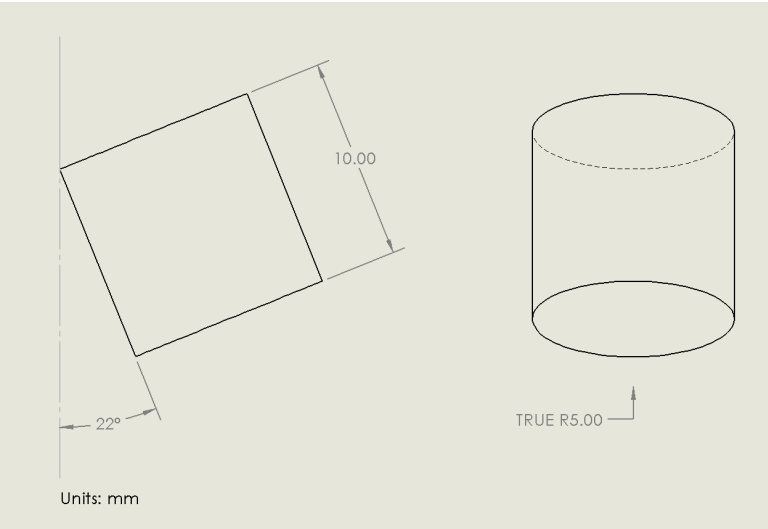

Figure 2: Dimensions of Cylinder Orifice (Nostril)

2.1.2 Computational Domain

The domain of the model is a 3D rectangular encasement around the oriented cylinder that represents a human nostril. The model employs an unstructured mesh with no biasing. Finer mesh controls are implemented on the cylinder, whereas a coarser face-sizing is used for the rest of the open domain. The 3D mesh consisted of 1,579,655 total finite volumes. A detailed depiction of the mesh domain can be seen in Figures 3 and 4.

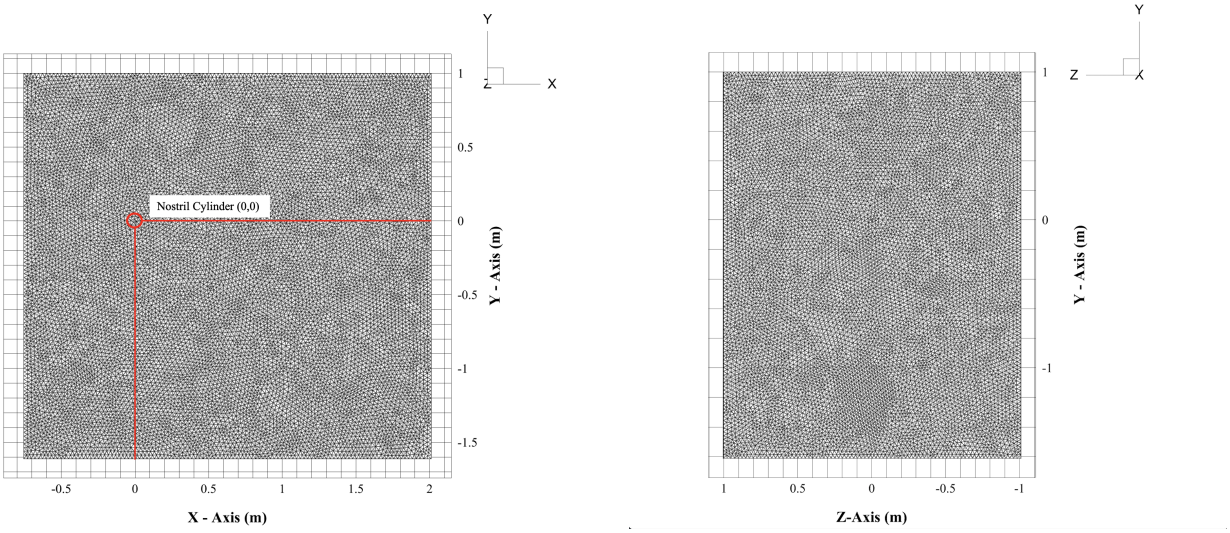

(a) XY Axis View of Mesh

(b) YZ Axis View of Mesh

Figure 3: Mesh Diagrams: XY and YZ View

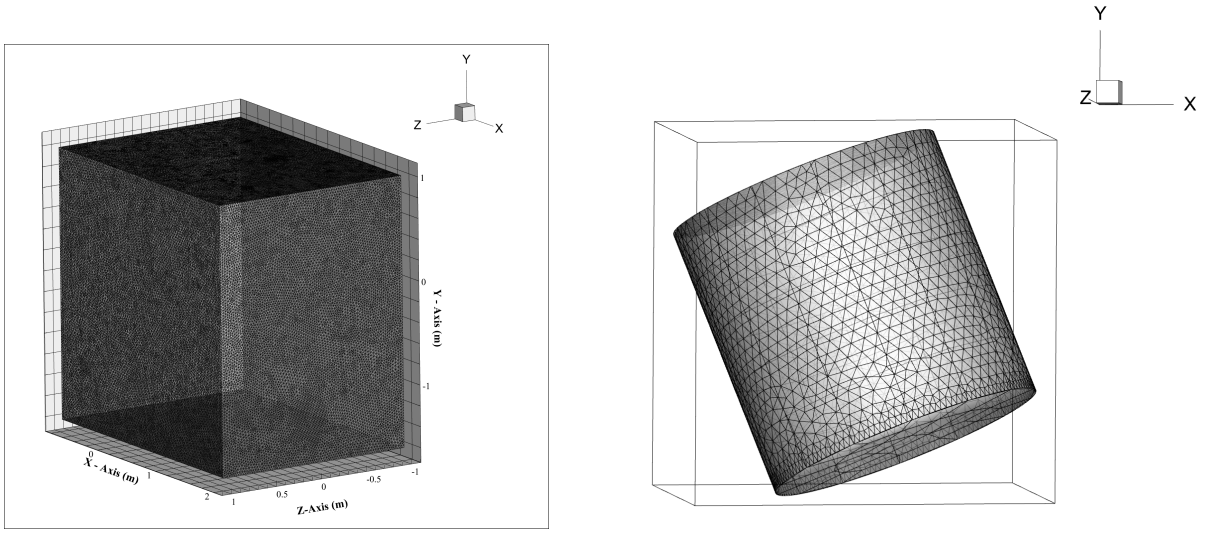

(a) XYZ Axis View of Mesh

(b) Cylinder Mesh

Figure 4: Mesh Diagrams: 3D View and Cylinder

To ensure the effectiveness of the mesh a grid sensitivity was performed which can be seen below in Figure 5. The parameters investigated for the grid sensitivity were mean XYZ position and velocity of the aerosols from all breaths at 11.4s of flow-time. Mean XYZ position and velocity were chosen as the grid sensitivity parameters seeing as they are the major parameters of interest regarding the aerosol behavior. The flow time of 11.4s was chosen because it is after 4 full breath cycles to allow aerosol trajectory development and is the midpoint of time simulated. The full range of mesh refinement study values are displayed in Table 1. The grid sensitivity results deemed it appropriate to choose the 1.5 million element mesh.

Number of Finite Volumes	X Position (m)	Y Position (m)	Z Position (m)	X Velocity (m/s)	Y Velocity (m/s)	Z Velocity (m/s)
392,006	0.212	-0.618	0.0018	0.023	0.021	0.0008
686,822	0.217	-0.175	0.0006	0.024	0.022	0.0001
1,001,814	0.221	-0.169	-0.0005	0.024	0.023	-0.0009
1,579,655	0.219	-0.168	-0.0046	0.023	0.024	-0.0009
2,421,628	0.219	-0.168	0.0013	0.025	0.023	0.0003
3,500,000	0.221	-0.171	0.00006	0.026	0.022	0.0003
4,500,000	0.223	-0.160	-0.0011	0.025	0.025	-0.0002

Table 1: Grid Sensitivity Values

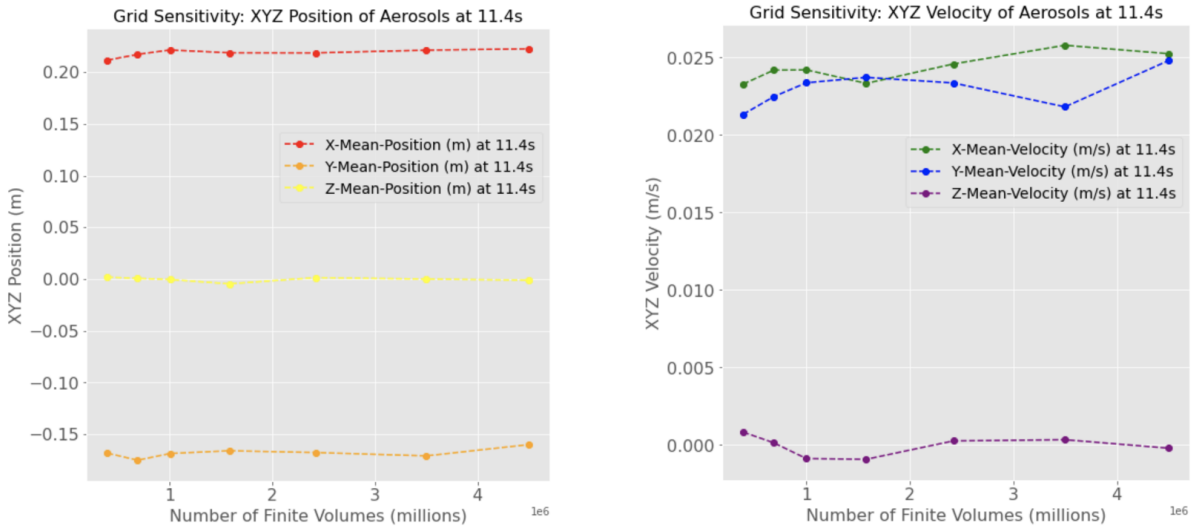

(a) Mean XYZ Position (m) at 11.4s

(b) Mean XYZ Velocity (m/s) at 11.4s

Figure 5: Grid Sensitivity Study

In order to confirm an appropriate time-step, a comparison was performed between a 0.1 and a 0.001 time-step. The parameters of interest compared were mean XYZ position and velocity after the first breath and rest period. The results can be seen below in Table 2, which confirms that the varied time-step has a minimal affect on results. The percent error remained below 9% save for the mean z position and velocity which are essentially zero which explains the large variance.

Parameter	0.1 Timestep	0.001 Timestep	Percent ERROR	Numerical Difference
Mean X Position (m)	0.06901	0.06355	8.23 %	0.00546
Mean Y Position (m)	-0.14902	-0.14039	5.79 %	-0.00863
Mean Z Position (m)	0.00147	0.00164	11.42 %	-0.00017
Mean X Velocity (m/s)	0.03244	0.02903	10.51 %	0.003411
Mean Y Velocity (m/s)	-0.05901	-0.05456	7.54 %	-0.00445
Mean Z Velocity (m/s)	0.00114	0.00053	53.76 %	0.000615

Table 2: Time-Step Comparison 0.1 to 0.001

2.1.3 Boundary Conditions

Figure 6 displays the boundary condition set-up for the simulation. The boundary conditions for the encasement surrounding the cylinder were all set to adiabatic walls with a no slip condition. The walls were set as traps with regards to particle interaction and the discrete phase model. The bottom of the cylinder is defined as a velocity inlet and serves as the face from which the aerosols are released and the flow enters the domain. This face is defined as an escape for particles in the domain which allows them to be eliminated if crossing the surface. The bottom of the cylinder serves to act as a human nostril during inactive breathing. The remaining faces of the cylinder are all set to no slip, adiabatic walls and also are defined as traps.

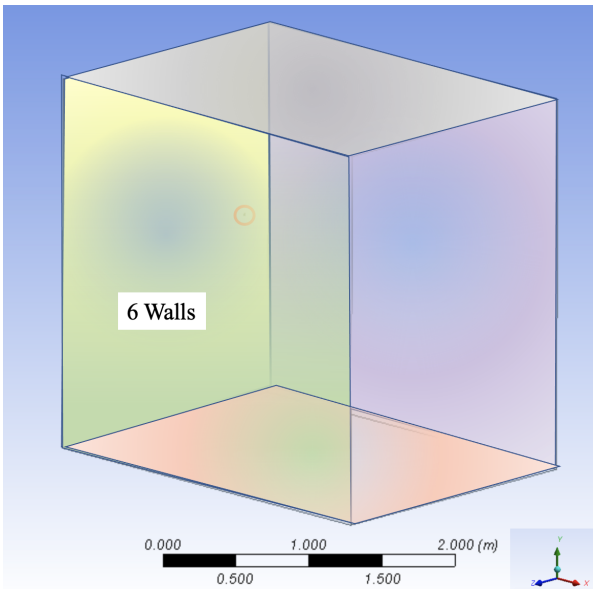

(a) Boundary Conditions for the Entire Domain

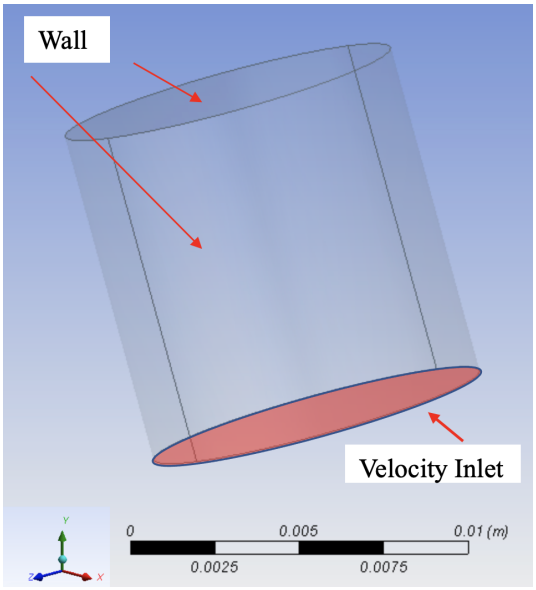

(b) Boundary Conditions for the Cylinder

Figure 6: Boundary Conditions

2.1.4 Numerical Methods

The following settings were used for the ANSYS RANS simulations as seen in Table 3. The Courant Flow Number (CFL) is defined as:

$$C \equiv \frac{u\Delta t}{\Delta x} \tag{7}$$

where u is the characteristic wave speed of the system and Δt is the time step of the numerical model and Δx is the spacing of the grid in the numerical model. It can be

considered a measure of how much information traverses a computational grid cell in a given time step. The time-integrator must have enough time to properly interpret what is physically happening within each grid cell, otherwise the solution is unstable and will most likely diverge. For scale-resolving simulations, the resolution of turbulent structures in time is essential.[6] As seen below, the convergence is adequate for the simulation with a high Courant number which allows for the desirable rapid simulations. Further theory behind each setting choice is further explained in the simulation methodology section. With respect to determining if the convergence of the simulation was accurate, the residuals are observed. The residual is the difference between the previous result and the current result. As these errors are decreasing the equation results are reaching values that are changing less and less.[5] This is what is known as convergence. The residuals of the simulation show good convergence below 1e-4 for all parameters as can be seen in Figure 7.

Solver	Pressure Based
Velocity Formation	Absolute
Time	Transient
Gravity: ON	-9.8 $\frac{m}{s^2}$
Turbulence Model	K-Epsilon
Species Transport Model	ON
Discrete Phase Model	ON
Pressure-Velocity Scheme	Coupled
Spatial Discretization	Gradient: Least Squares Cell Based Pressure: PRESTO!
Transient Formulation	First Order Implicit
Time Step Size	0.0285
Time Step Number	700
Max Iterations per Time Step	75
Flow Courant Number	200

Table 3: Numerical Methods Information

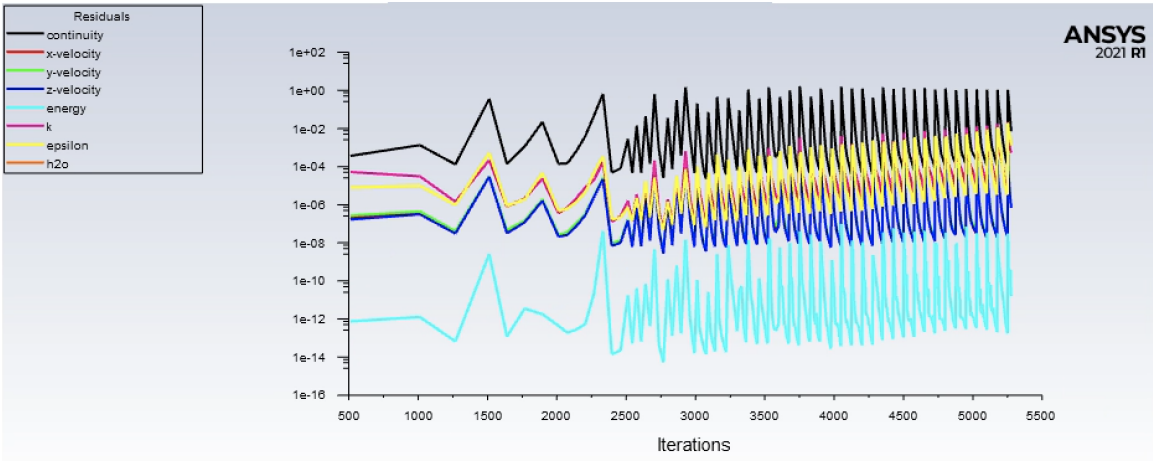

Figure 7: Residual Convergence

2.2 RANS Simulation Methodology

2.2.1 Initial Conditions

The simulation is intended to replicated nose-breathing as closely as possible. A simplified domain of one nostril (modeled as a cylinder) is used as a velocity inlet as described in the physical model section. One nostril was used to keep the simulation as simple as possible at first but should be upgraded to two nostrils moving forward. The height of the nostril is located 1.6m and produced a downward facing jet at twenty two degrees from the vertical. A breathing waveform is implemented as a velocity inlet that has a breath cycle of 2.85 s. The exhalation lasts from 0s to 1.8s which is followed by 0.15s of zero velocity as a breathing pause. Usually this would be followed by a 0.9s inhalation period, however the inhalation

profile has been set to 0 velocity for this simulation to keep simplicity. Due to the similarities in results of the high fidelity code, which accounts for inhaling, it can be considered within reason to not include inhalation for the most simplistic of studies. Therefore the breathing waveform represents the exhalation with a set velocity profile, followed by a pause and time representative for an inhalation period of zero velocity. The nose-breathing waveform can be seen in Figure 8. The simulation covered 8 total breath cycles, to allow equal analysis of 4 breaths through a period of 11.4 seconds. The parameters under investigation are the mean X, Y and Z position as well as velocity of the aerosols from their release up until 11.4 seconds later.

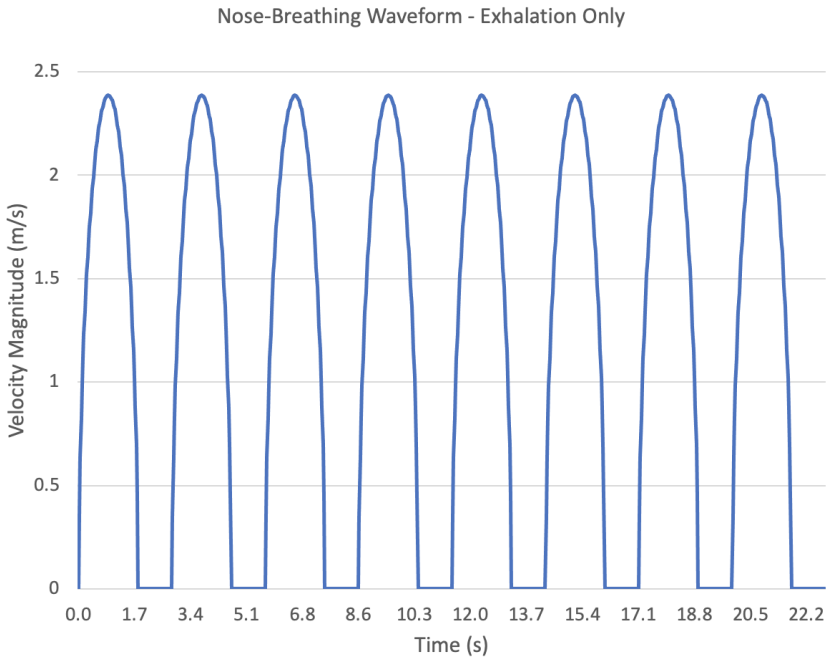

Figure 8: Nose-Breathing Waveform

To properly simulate the humidity of a nose-breath the ANSYS Fluent species transport model is employed for the gas phase which consists of air and steam. The jet leaving the nostril exits at a temperature of 308.15K with a mass fraction of H_2O of 0.012 to represent the greater temperature and humidity assumed.[15,16] The ambient air in the chamber was assumed to be at 293.15K.

2.2.2 Droplet Tracking Model

In order to model the aerosols in ANSYS Fluent, a discrete phase model was implemented. Uncoupled or one-way coupling was deemed adequate as the discrete phase (aerosols) is at a low mass and momentum loading. Therefore the continuous phase is not influenced by the presence of the discrete phase and two-way coupling is not necessary. The discrete phase model uses unsteady tracking with a 10,000 as the max number of time-steps and 10 as the step length factor. As for numerics, the accuracy control is set with a tolerance of 1e-05 for calculations with regards to tracking. The number of max refinements, which is the maximum number of step size refinements in one single integration step, is set to 20. The tracking scheme is trapezoidal for high order while the low order scheme is implicit.

Four injections were used in junction with this model to represent the four breaths that would be analyzed. All injections contained the same properties with respect to modeling the aerosols. The aerosols assumed to have already reached a smaller diameter due to

evaporation and are modeled with a 0.1 micron diameter. The aerosols are modeled as inert H_2O particles due to the negligible affect of gravity at such a minimal diameter. The mass flow rate of the injected particles is 9.410e-15 kg/s which is much greater than the actual viral load that would be emitted. However, due to the minimal amount of aerosol mass compared to gas phase, and therefore minimal influence of the discrete phase, it was deemed appropriate to inject more mass in order to better visualize their distribution. An average nose breathing flow rate could be considered 7.516e-4 kg/s.[10] For the simulation the flow rate is per each element upon the release surface which is why it is so drastically reduced. The aerosols are released at a temperature of 300 K. The particles are injected from the bottom of the cylinder at the same location where the main flow is released and follow the velocity profile for injection timing. Particles are injected during the exhalation period, but not during the time period that represents inhalation or the rest period, each where the flow velocity is equal to zero. Injections are present only for four breaths as to simulate more breaths for the same amount of time each the simulation would have had to have been run for a longer amount of time. Due to the lack of influence of the aerosols on each other, it was appropriate to omit particles for the remaining four breaths. The injection release timing for each breath is outlined below in Table 4.

Breath Number	Duration of Total Breath Cycle (s)	Particles Injected?
1	0s - 2.85s	Yes (0s -1.8s)
2	2.8785s - 5.7s	Yes (2.8785s - 4.6455s)
3	5.7285s - 8.55s	Yes (5.7285s - 7.4955s)
4	8.5785s - 11.4s	Yes (8.5785s - 10.3455s)
5	11.4285s - 14.25s	No
6	14.2785s - 17.1s	No
7	17.1285s - 19.95 s	No
8	19.9785s - 22.8s	No

Table 4: Breath Structure

The spherical drag law is implemented to account for drag on the aerosols which is defined in Equation 8, where a_1, a_2 and a_3 are constants that cover a range of Reynolds numbers.

$$C_D = a_1 + \frac{a_2}{Re} + \frac{a_3}{Re^2} \tag{8}$$

The discrete random walk model is also employed to include the effect of instantaneous turbulent velocity fluctuations on the particle trajectories through the use of stochastic methods.[1] Discrete phase particle trajectories are predicted by integrating the force balance on the particle which is written in a Lagrangian reference frame as seen in Equations 9-11.

F_x is an additional acceleration term that is further defined below as it can be important in certain instances.

$$\frac{du_p}{dt} = F_D(u - u_p) + \frac{g_x(\rho_p - \rho)}{\rho_p} + F_x \tag{9}$$

$$F_D = \frac{18\mu}{\rho_p d_p^2} \frac{C_D Re}{24} \tag{10}$$

$$Re \equiv \frac{\rho d_p |u_p - u|}{\mu} \tag{11}$$

The "virtual mass" force is the force required to accelerate the fluid surrounding the particle and can be written as:

$$F_x = \frac{1}{2} \frac{\rho}{\rho_p} \frac{d}{dt}(u - u_p) \tag{12}$$

This is important when $\rho > \rho_p$, as an additional force arises due to the pressure gradient in the fluid:

$$F_x = \frac{\rho}{\rho_p} u_{pi} \frac{\partial u}{\partial x_i} \tag{13}$$

The Discrete Phase Model is used for droplet tracking as the position and velocity of the aerosols throughout the breath cycle are of great interest. The mean XYZ position is investigated at different times in order to understand the trajectory of the particles over time as breathing continues. The effect of continued breathing on the aerosol location is considered to better understand the behavior of the aerosols due to continued nose-breathing, and how

their motion may reach an equilibrium. In addition to position, the mean XYZ velocities of the aerosols are measured throughout the analysis to allow for understanding regarding the evolution of particle movement.

3 Results

3.1 Mean XYZ Position and Trajectory

3.1.1 Qualitative

It is first important to understand visually how the nose breath evolves. In order to provide the most informative visual demonstration of particle dispersion, two qualitative Figures (9 and 11), that display different points in time are supplied. The two flow times chosen are 11.4s and 19.95s, as these are after the fourth and eighth breaths have been simulated. This allows each breath, 1-4, to have been present for 11.4s to allow ample time for dispersion. In Figures 9 and 10, the nostril is located at (0,0,0) and the XYZ position of particles released from 0 - 11.4 s can be visualized. The particles are colored by residence time as seen in the color bar on the right. Residence time is how much time has passed since the particle was released, or in other words, how long the particle has been present in the domain. From the XY axis perspective, it is clear that that the particles have an initial downward trajectory, but at around -0.35m, begin to curve upwards as the initial negative

y-velocity dissipates and buoyant forces prevail. In this time the particles have reached a position about 0.4 m from the nostril in the x-direction, but as the particles begin to rise this x-oriented movement is slowed. However at 11.4s only a minimal amount of the aerosols in the first breath released have risen to the y-position where the nostril where they were first released, and the majority of the particles remain below the nostril. In Figure 10 (b), the dispersion along the z-Axis reaches about 0.2m from the nostril on either side.

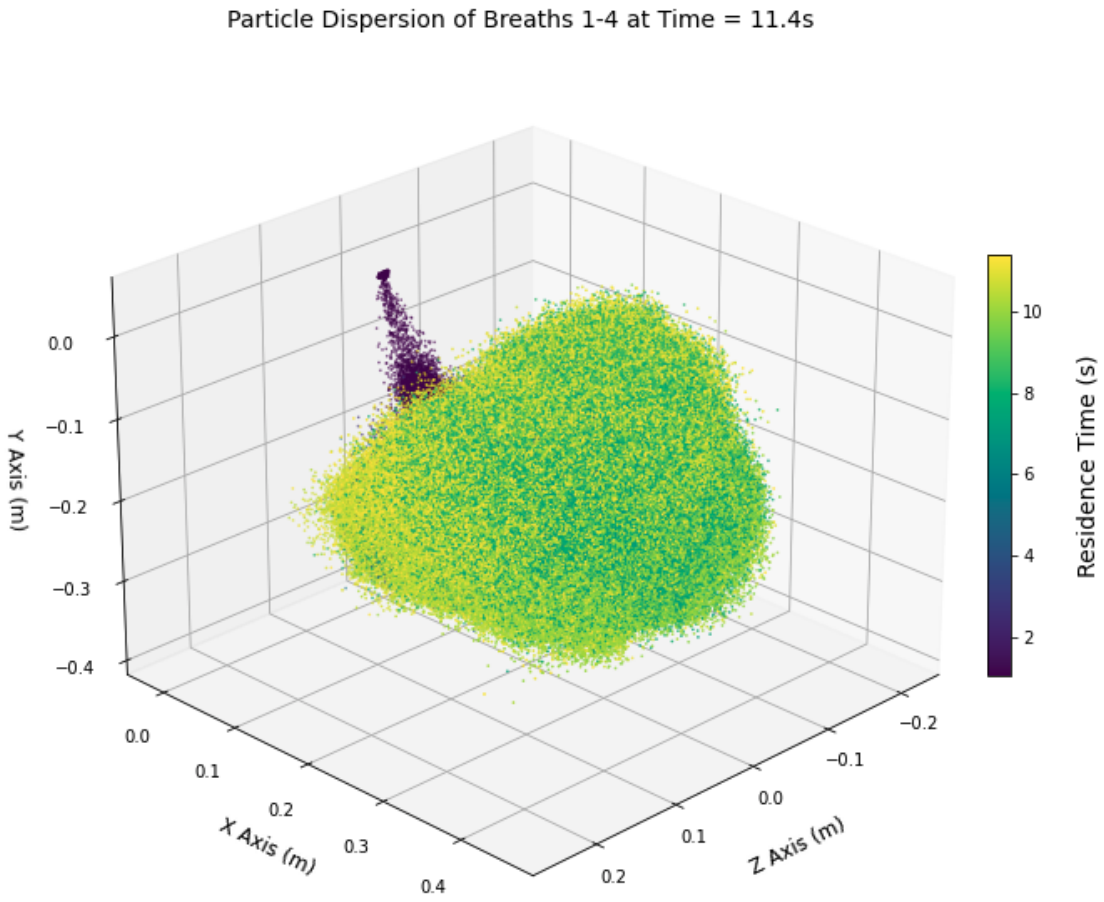

Figure 9: XYZ Position of Aerosols at 11.4s

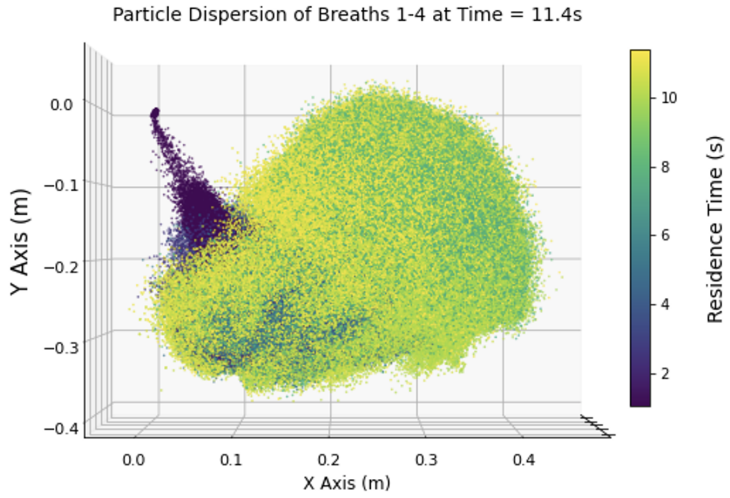

(a) XY Axis Perspective

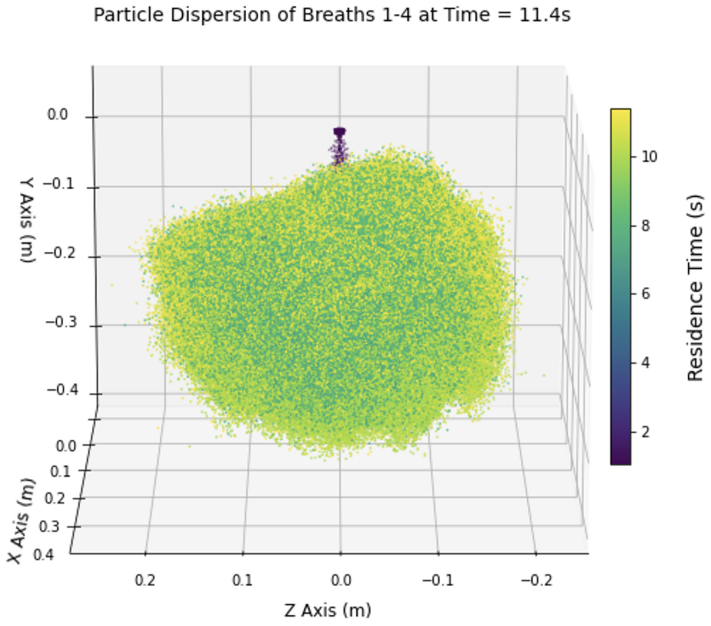

(b) Z Axis Perspective

Figure 10: Particle Dispersion 11.4s XY and Z Axis Perspective

In Figures 11 and 12 the particle dispersion can be seen at a time of 19.95s. At this point, the rising motion of the particles from breaths 1-4 can clearly be visualized. The majority of particles have now risen above the nostril at (0,0,0) and have reached as far as 0.4m above the release position along the y-axis. The last particles to be released at around 10s, (shown in dark purple), are just finishing their downward journey and beginning the rise as demonstrated by the residence time coloring. Although the bulk of aerosols remain located at a distance of 0.35 m from the nostril along the x-axis, the edge of the particle cloud reaches as far as 0.6 m horizontally from the release position. Along the z-axis, the width distribution has only increased slightly from 11.4s to 19.95s, just passing the 0.2 m mark from either side of the nostril.

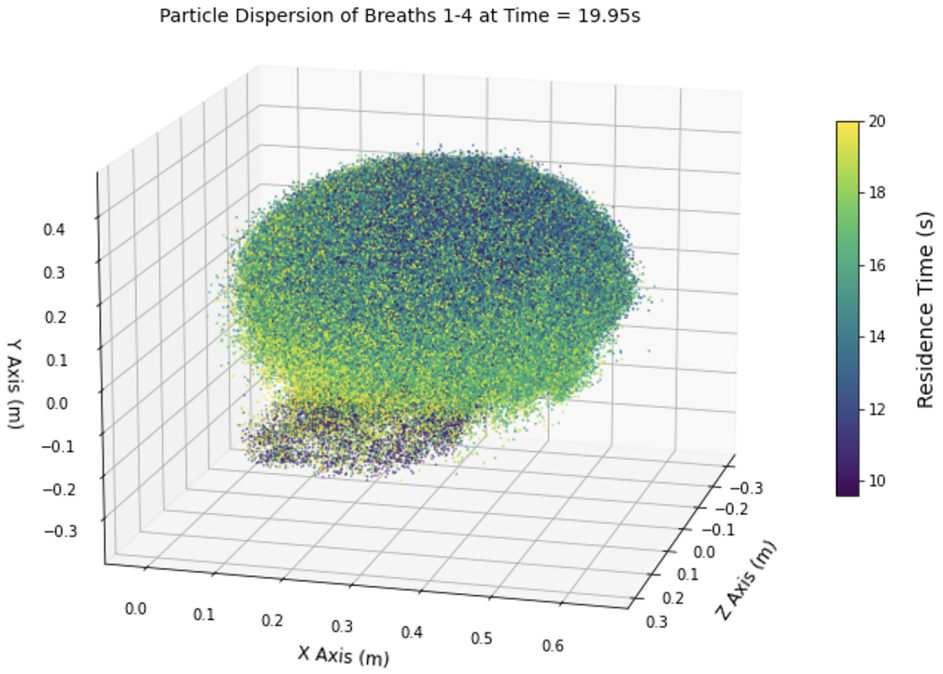

Figure 11: XYZ Position of Aerosols at 19.95s

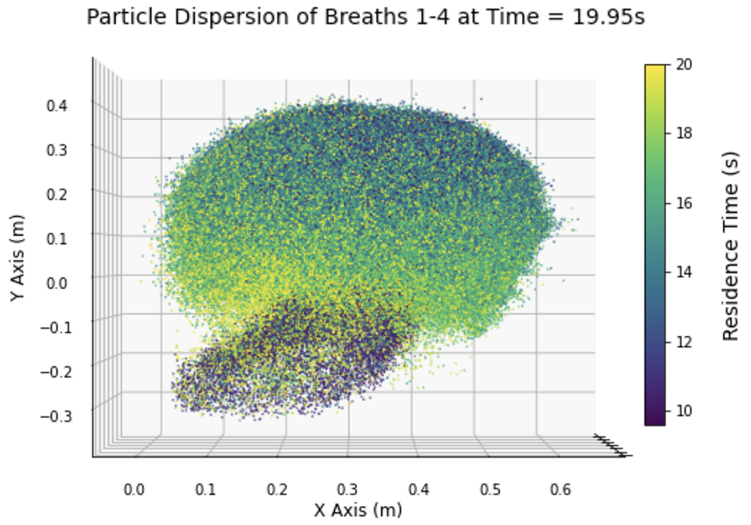

(a) XY Axis Perspective

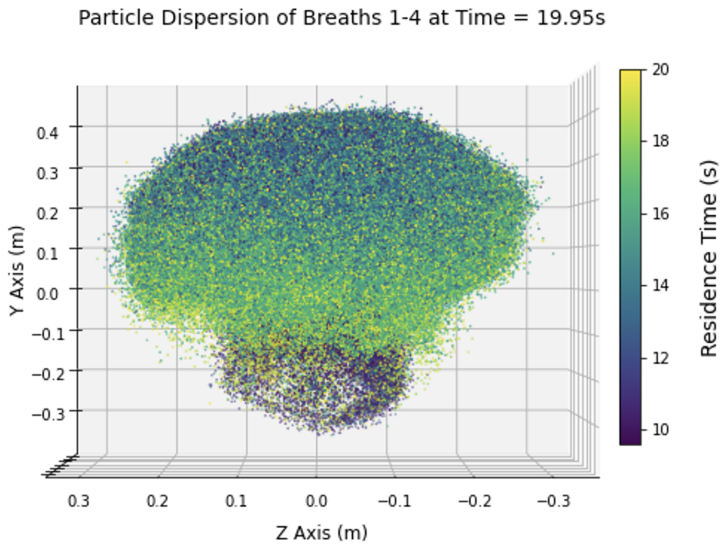

(b) Z Axis Perspective

Figure 12: Particle Dispersion 19.9s XY and Z Axis Perspective

3.1.2 Quantitative

In order to properly quantify the position and velocities of the aerosols the average of the quantity of interested was observed. At the end of each breath, so in this case breaths (1,2,3,4) the mean of the parameter of interest, is taken of all the particles attributed to that breath at that point in time. For example, looking at mean position, for each point seen on the graph, the mean position of the particles corresponding to the specific breath was taken and then plotted over time. In Figures 13, the mean x and y position were then plotted versus flow-time so that the behavior of the aerosols from breath to breath could be analyzed. Figure 13 (b) of y-position includes data taken from the YALES2 code to allow for a comparison. Regarding x-position, at 11.4s the aerosols have reached a position between 0.27 and 0.37 m from the nostril. The first breath aerosols do not travel as far and as the subsequent breaths, however, the x-position of breaths 2, 3, and 4 are more precise and approach a similar value. The mean y-position of aerosols has a wider distribution of values, ranging from nearly -0.3 m to 0.25m. Although the difference in y-position values is greater between breaths, the difference does follow the same trend as x-position and gets smaller from breath to breath. This reduction in difference between breaths suggests that the data is approaching an equilibrium. The x and y position mean values match the visual distribution of aerosols seen earlier which serves as a check for both data sets. The YALES2 simulation has been run for more breaths than the ANSYS RANS simulation, which is why

the yellow line representing the YALES2 comparison is breaths 1-4 averaged, and the orange line is the YALES2 breaths 4-15 averaged.

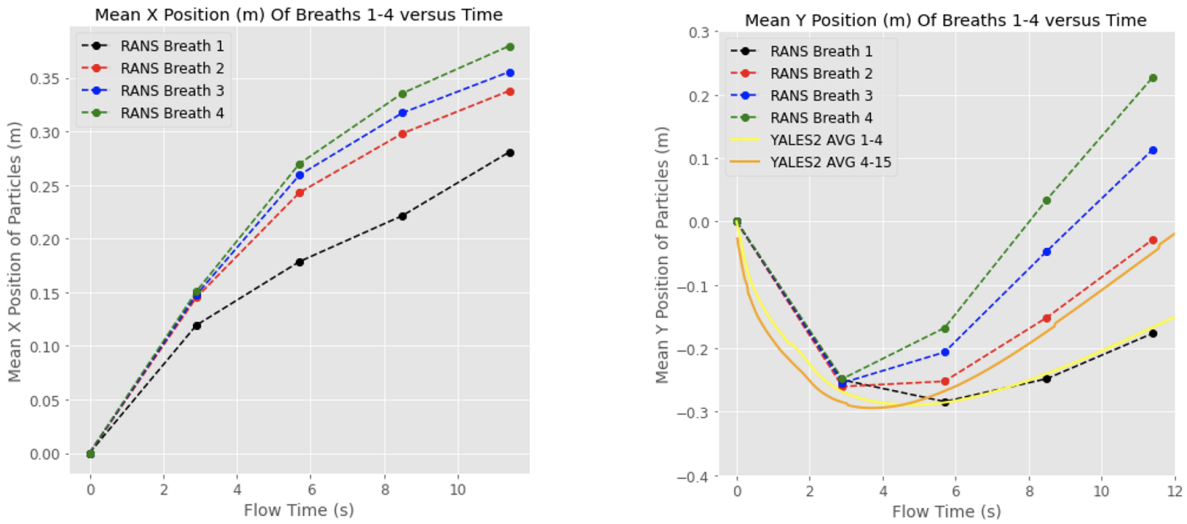

(a) Mean X Position (m)

(b) Mean Y Position (m)

Figure 13: Mean X and Y Position of Aerosols From Each Breath at 11.4s

Figure 14 provides a visualization of the mean XYZ positions as a trajectory in 3D space. The 3D trajectory serves as a representation of all the positional distributions discussed above.

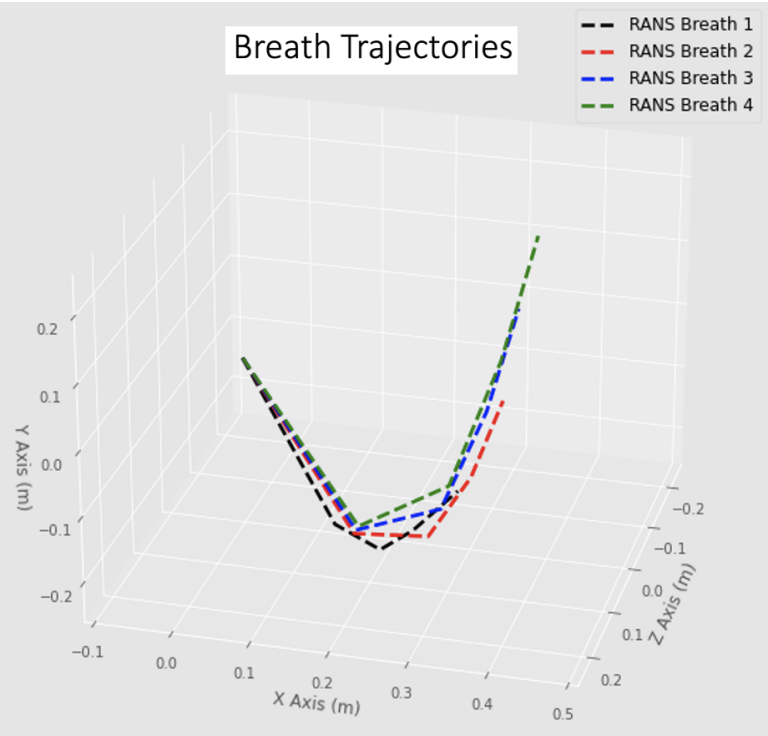

Figure 14: Breath Trajectories of Breaths 1-4 after 11.4s

3.2 Mean XYZ Velocity

Figure 15 displays the mean x and y velocity of the particles for all 4 breaths over 11.4s. The x-velocity of the aerosols increases as they are released from the nostril for about 6s, where it begins to decrease. The mean x-velocity for all four breaths shows great precision with extremely close values at time = 11.4s. At this point in time, the x-velocity has slowed to nearly 0.01 m/s as the main trajectory of the particles transitions from horizontal to vertical movement. Regarding mean y-velocity which also shows the YALES2 comparison,

the aerosols keep a negative velocity for about 3s until they being to rise with a linear increase of velocity to about 8.5 seconds. After this point, the y-velocity of the aerosols begins to plateau and hold a constant value between about 0.04 m/s and 0.08 m/s for the ANSYS RANS results. 0.04m/s can be considered a fairly significant difference in aerosol y-velocity from breath one to breath four. The YALES2 results reach a y-velocity plateau at a lower value of about 0.035 m/s.

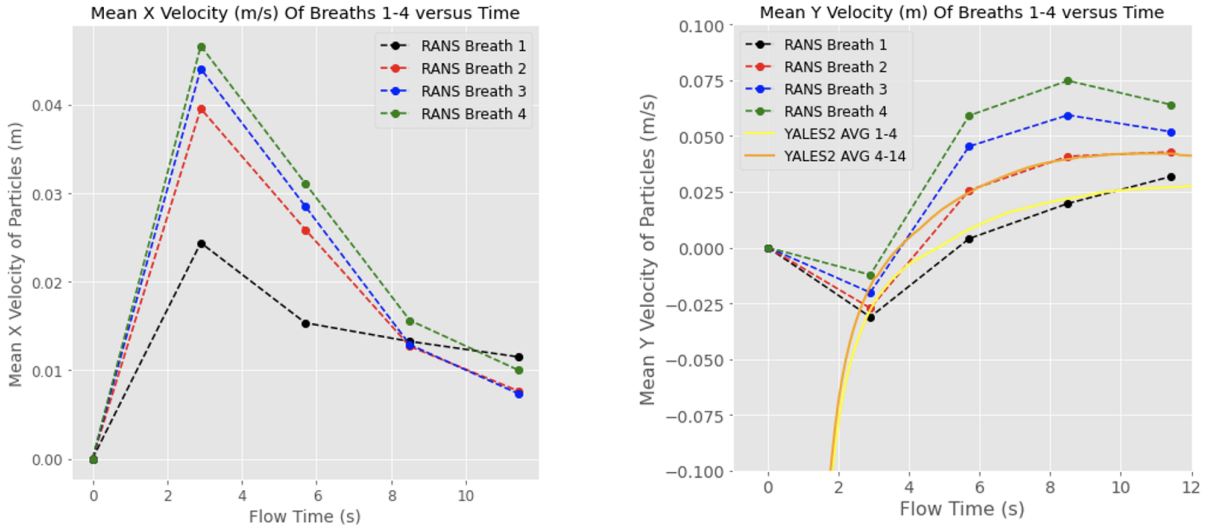

(a) Mean X Velocity (m/s)

(b) Mean Y Velocity (m/s)

Figure 15: Mean X and Y Velocity of Aerosols From Each Breath at 11.4s

3.3 Binning By XYZ Position

Predicting aerosol behavior is a crucial part in understanding transmission risk, and in order to do so, the concentration of aerosols within range of the mouth and nose must be well quantified. Figure 16 shows a 0.4m by 0.4m by 0.4m cube that represents what could be considered an area of high inhalation risk due to the proximity to the nose and face. By categorizing how many aerosols lay within the 3D space surrounding where inhalation risk is increased, a greater understanding of transmission risk can be made. Figures 17 and 18 display the xy and z axis perspectives of aerosols that fall into the increased chance for inhalation area. It was found that 83,397 of 1,006,188 aerosols, or 8.288% at time 11.4s were within the region of increased inhalation. At 19.95s, it was found that 73,044 of 1,006,184 aerosols, or 7.260% of aerosols were in the region of greater inhalation risk. At 11.4s although the majority of particles are within the defined 3D space along the z-axis, the aerosols are propelled far enough in the x-direction away from the nostril that only a small percentage fall within the area of increased inhalation risk. At 19.95s not only are the majority of the particles beyond the x-axis defined limit, but they have risen above the nostril and away from the area of higher inhalation risk.

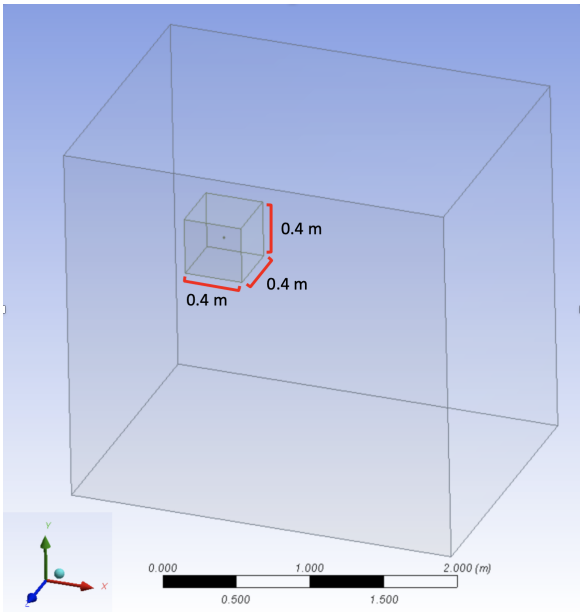

Figure 16: Inhalation Risk Area

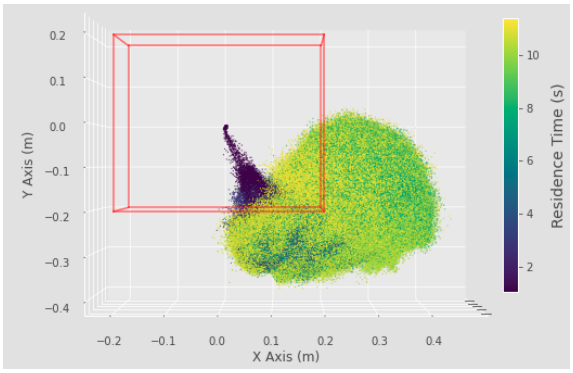

(a) XY View Bin Aerosols - Inhalation Region

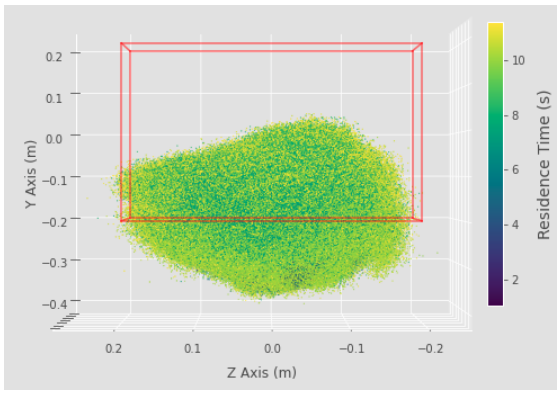

(b) Z View Bin Aerosols - Inhalation Region

Figure 17: 3D Binned Aerosols - Inhalation Region at 11.4s

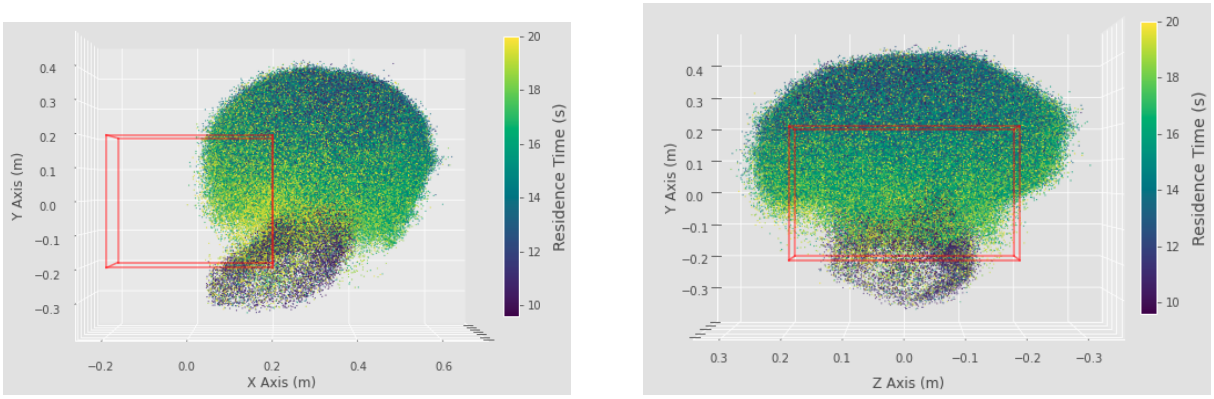

(a) XY View Bin Aerosols - Inhalation Region

(b) Z View Bin Aerosols - Inhalation Region

Figure 18: 3D Binned Aerosols - Inhalation Region at 19.95s

The visual of increased inhalation risk area is quantified below according to x, y, and z position in Figures 19, 20, and 21. The charts allow aerosol density totals based on 0.1m increments from the nostril in each direction (XYZ) at 11.4s and 19.95s. As expected for x-position, the majority of the particles lay 0.1m to 0.4m away from the nostril at 11.4s. By 19.95s the particles have traveled further and the majority now lay within the 0.2m to 0.6m region. For y-position at 11.4s the majority of particles are still located below the nostril, but at 19.95s the expected trend upward is visualized as the density of particles above the nostril is much greater, laying in the 0.1m to 0.5m region above. Lastly, for z-position the distribution of aerosols at 11.4 and 19.95s are nearly equivalent as expected due to the limited travel along the z-direction between 11.4 and 19.95s.

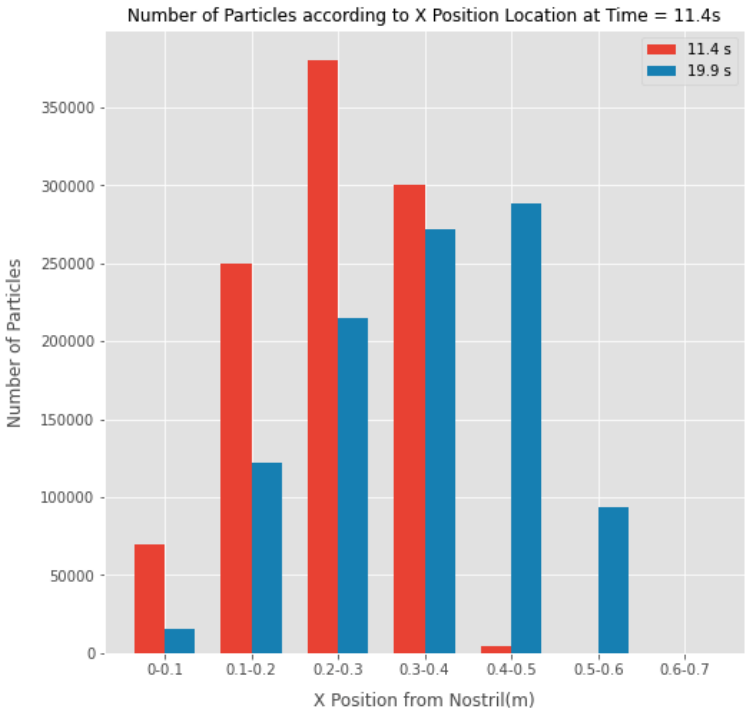

Figure 19: Binned Particles According to X Traveled Distance (m)

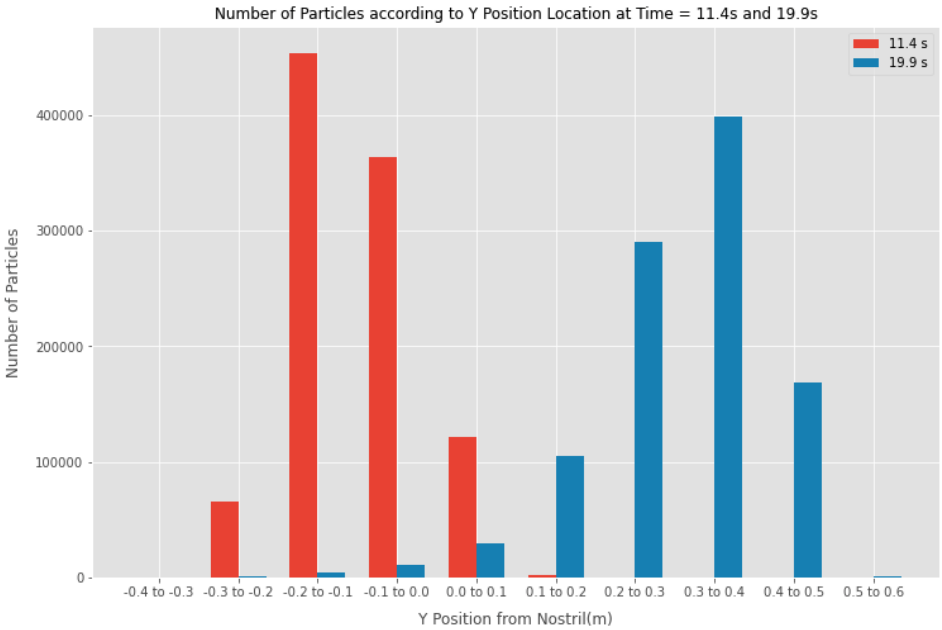

Figure 20: Binned Particles According to Y Traveled Distance (m)

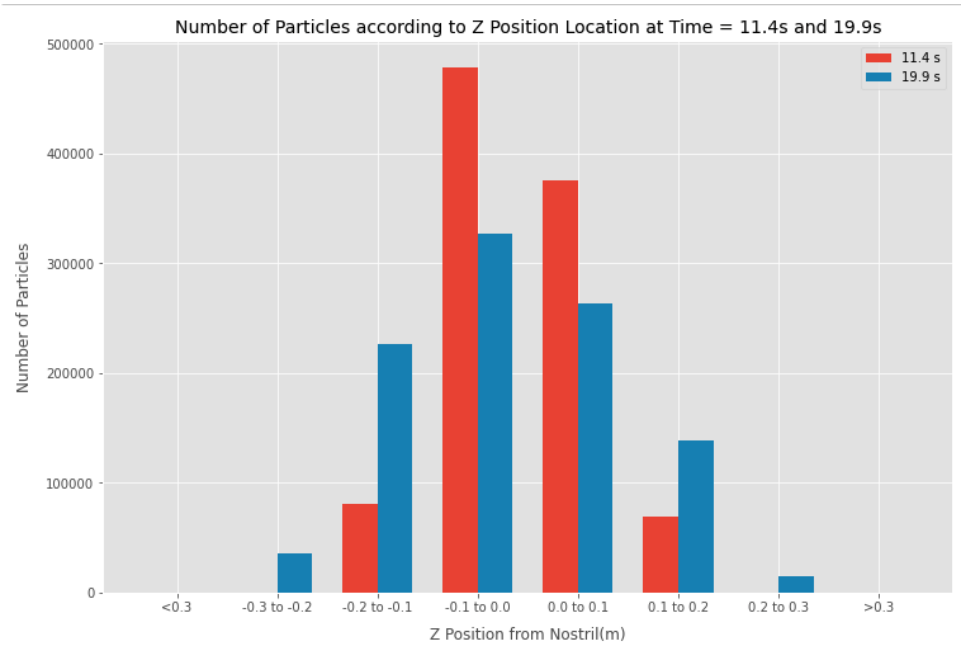

Figure 21: Binned Particles According to Z Traveled Distance (m)

4 Discussion

The goal of this project intended to better understand the limits when it comes to using a lower fidelity simulation software such as ANSYS Fluent in accurately modeling the dispersion of aerosols at lower Reynolds numbers. Although high fidelity computational software provides unmatched accuracy, this comes at the price of complexity and high computational demands in time and power. The RANS methodology demonstrated by by ANSYS Fluent within these simulations has proven to be sufficient in reproducing qualitative aspects of the YALES2 results with regards to the dispersion behavior of aerosols from a low velocity ac-

tivity such as nose breathing. The first parameter investigated was the aerosol XYZ position as it evolved over time. The most notable aspect here is the curved trajectory of the aerosols as the buoyant forces dominate over gravitational forces and the original negative velocity. A mere 20 seconds after being released the majority of aerosols have risen above their point of release. These aspects were demonstrated by the lower fidelity code, however much work remains to be able to place confidence in using low fidelity simulations in junction with high fidelity simulations.

4.1 X and Y Position Discussion

When observing the how the aerosols disperse in the 3D space, there is a clear trajectory path that differs slightly breath to breath. The mean x-position of the aerosols become closer in value after 11.4s with each breath. This suggests that an equilibrium with respect to the x-direction is starting to form. Although the difference in mean y-position at 11.4s is greater between breaths when compared to x-position, the difference is reducing in value as the breaths continue. Therefore similar to x-position, the mean y-position data suggests that as breaths continue an equilibrium with respect to y-position is developing. The importance of an equilibrium with respect to positional parameters is two fold. The first being that the previous and future breaths that a person has or will release greatly effect the positional placement of the aerosols. As seen with the x and y positions, breath exhalations that have

been in the ambient environment for the same amount of time show not only different final positions, but values that are increasingly closer together. The second being that, if more breaths are simulated and the behavior indeed does reach some type of equilibrium, it will aid in predicting long term behavior of the dispersion that otherwise may have been more complex. Although qualitatively the YALES2 trend lines correspond somewhat well to the RANS simulation, it can be seen that with triple the amount of breaths, the YALES2 aerosols are not rising as high as the RANS simulation of a mere four breaths. This suggests that the ANSYS RANS simulation is overshooting the speed and distance at which the aerosols are traveling which will be explored in more detail when discussing y-velocity behavior.

4.2 X and Y Velocity Discussion

Similar to the XYZ positional investigation, a likewise phenomena can be witnessed when observing the XYZ mean velocities. In this case, the mean x-velocities all approach a value of 0.01m/s, nearly zero, by the time 11.4s has passed. This can be attributed to the dissipation of x-velocity provided from the release, as well as the change in direction of velocity from in the positive x direction to the positive y direction. By observing the mean y-velocities, a better understanding can be developed that relates it back to the x-velocity. The RANS mean y-velocities appear to plateau for each breath on a range of 0.04m/s to 0.08 m/s at the same point that the x-velocity is reduced to nearly zero. This is expected as

the particles are no longer propelled forward but are rising vertically due to buoyancy. The rise in mean y-velocities from breath to breath suggests that the previous breath entrains the incoming breath and causes the aerosols to rise faster. This phenomena can be thought of as a continuation of momentum from the previous breath. It is unclear after four breaths whether or not the vertical velocities of the aerosols are reaching an equilibrium from breath to breath from the RANS simulations.

It is important to address the greater magnitude of negative y-velocity that the YALES2 results appear to be presenting from 0-2 seconds that the ANSYS RANS results are not showing. This is most likely is a result of insufficient data point collection on the RANS side of things. If a greater number of data points were taken between 0 and 2 seconds, we would most likely get these greater negative y velocity values from the RANS as well. We can see from the YALES2 values that they reach a plateau or constant vertical velocity around 11 seconds at a value of just below 0.05 m/s. However as mentioned before the mean y-velocities for RANS appear to begin to plateau for each breath on a range of 0.04 m/s to 0.08 m/s. The lower vertical velocities seen in the YALES2 results can most likely be attributed to the ability of the YALES2 code to properly simulate smaller scales of turbulent mixing. This will allow for the hotter nose jet to dissipate quicker into the ambient environment, therefore lowering the kinetic energy of the aerosols and resultingly the velocity of the aerosols. With RANS it can be hypothesized that these smaller scales of mixing are not properly modeled,

and therefore the aerosols have a higher kinetic energy from the breath and therefore a greater vertical velocity magnitude at later points in time.

4.3 3D Binning Discussion

The concentration of aerosols throughout time is an important parameter under investigation. By characterizing the areas of high aerosol density, stronger predictions related to inhalation and transmission can be made. As stated in the results section, an extremely low percentage of aerosols were within the 0.16 m^2 space defined as great inhalation risk. From the aerosol dispersion patterns and predicted equilibrium behavior, the data suggests that the aerosols will continue to rise out of the area of greater inhalation risk as time progresses. The following figures that show the distance traveled in the X, Y and Z directions also support the findings. In the x-direction the aerosols at 11.4s have traveled mostly to 0.4m, but at 19.95 seconds they have progressed past this out to 0.6m. This shows that the majority of aerosols at 11.4s travel about double the x distance to 19.95s. The y-distribution gives a great visual as to how at 11.4s the aerosols certainly have risen, but at 19.95 s the aerosols have continued to rise much further. As expected the Z-axis distribution is fairly symmetrical as no angle in this axis was applied. It is important to keep in mind there are many important factors are not considered in this study that may further impact aerosol concentration around the head. One of these factors directly affecting the concentration of

aerosols around the nostril is the inhalation force. The effects of inhalation were omitted from this study and replaced with zero velocity to keep simplicity. As a result, the effects of inhalation may entrain a greater number of aerosols closer to the nostril. In order to gain more confidence in these results, additional breaths should be simulated as well as the effect of inhalation, to confirm the predicted behavior surrounding the nostril.

It is important to keep in mind that the simulation at hand assumes employs many simplifications and assumes specific ambient conditions. As previously mentioned, no profile is implemented for inhalation, only exhalation. The ambient conditions of the room do not account for any external turbulence which would not be encountered in everyday life, even in what appears to be a "perfectly still" environment. The enclosed space also is set for a mild temperature and humidity, alterations of these parameters may affect the aerosol behavior. Overall, the results produced by the ANSYS RANS simulation suggest that the lower fidelity software can offer valuable information in short time and is worth further investigation for the lower Reynolds number situations such as nose breathing. In other words, the simplifications must be kept in mind with regards to the modeling of aerosol dispersion.

5 Conclusions

Fluids simulation software, akin to much else in the computational world, exists on a spectrum of complexity. Lower fidelity software is attractive due to its ability to provide rapid results at a reduced cost of computational time as well as handle a wide range of situations. However, as touched upon throughout this paper, the streamlined approach comes at a cost. Generally, this is a result of averaging smaller value fluctuations and frequent use of more elementary equations that may not properly model all aspects of the physics of the flow. In a quickly evolving world however, the use for rapid simulations can be of critical need. Therefore it is crucial to understand the limits of lower fidelity software on a situation basis by comparing it to higher fidelity results. This allows for greater confidence in when lower fidelity software can and cannot be accurately applied. The COVID-19 pandemic is stands as an example where early and accurate characterization of dispersion behavior could have helped define effective safety guidelines. As the pandemic begins to change form, a greater investigation into everyday situations such as nose breathing is important to consider.

The following ANSYS Fluent simulation utilized RANS methodology in order to model the dispersion of aerosols in a low Reynolds number situation. The results suggest that the surrounding breaths can greatly affect the distribution of aerosols. In other words, this means that continued breathing affects the behavior of aerosols as their behavior adjusts breath to breath as it reaches equilibrium with the ambient environment, therefore multiple

breaths must be simulated for greater accuracy. From this perspective, future predictions can be made with more confidence compared to if a equilibrium did not look evident. A possible tool was investigated that quantified the concentration of aerosols surrounding the nostril at different points in time in an attempt to gain understanding regarding inhalation or transmission risk in this situation. This 3D binning method shows promise for use as a tool in identifying areas of high aerosol concentration. As seen with vertical position and velocity the quantitative differences show that the ANSYS RANS simulation is far from completely matching the YALES2 direct numerical simulation. RANS overshot the vertical velocity and positioning most likely do to the lack of turbulent mixing as described earlier. Despite these discrepancies, the RANS ability to reproduce similar qualitative results to the high-fidelity simulation suggest value in continuing to pursue the use of multi-fidelity CFD. By continuing to fine-tune the RANS modeling of the physics as best as possible, this study provides evidence that a low fidelity code used in junction with a higher fidelity code, could certainly offer increases in computational efficiency.

6 Future Work

Despite the comprehensiveness of this study there are many areas for future work regarding this subject matter. As always, simulating a greater number of breaths would help

install more confidence in results with regards to the breath to breath behavior patterns. With regards to the physical domain, it would be beneficial to include a human body and head just to account for any possible effects on the flow and to provide more of a visual. With respect to the simulation set up, there are a couple aspects that could be improved moving forward. This includes implementing adaptive mesh refinement to ensure better definition of smaller scales of turbulence and a general increase in accuracy. Moving forward it would also be beneficial for the nose breath to be released and develop within a cylinder that represents the geometry of a nostril before entering the domain. Releasing the nostril jet from the flat cylinder may not allow the flow to develop and take its proper form. Regarding the simulation itself, there are many more factors to introduce to the simulation in order to test its abilities. Small amounts of turbulence should be introduced as well as low wind velocities to see how the aerosol dispersion is affected. This may also include expected ventilation patterns. Other disruptive factors that should be investigated are sources of heat commonly found indoors that may have convective effects, such as humans or light sources.

7 Acknowledgements

Throughout my honors thesis research I have received guidance and support from a number of faculty and students at UVM. First and foremost I would like to acknowledge my

thesis advisor Dr. Yves Dubief. His continued inspiration and enthusiasm kept this project on the leading edge of COVID-19 computational fluid modeling. Not only did his guidance and motivation help me in navigating this project, but my future in fluid dynamics as a whole. I would like to thank Soham Banerjee for his continued assistance in trouble shooting and debugging of computational efforts to utilize the VACC. Dr. William Louisos was of great assistance with regards to direction and the use of ANSYS Fluent software. I would also like to thank Dean Linda Schadler for her assistance in direction and guidance throughout the project as well. Lastly, I would like to thank the Vermont Advanced Computing Core for their provided facilities to aid in computational efforts.

References

[1] "ANSYS FLUENT 12.0 Theory Guide - 4.5.1 Standard - Model." https://www.afs.enea.it/project/neptunius/docs/fluent/html/th/node66.htm (accessed Dec. 02, 2020).

[2] "ANSYS FLUENT 12.0 Theory Guide - 15.2.1 Equations of Motion for Particles." https://www.afs.enea.it/project/neptunius/docs/fluent/html/th/node241.htmeq9.2.1 (accessed Mar. 28, 2021).

[3] B. E. Launder and D. B. Spalding, "The numerical computation of turbulent flows,"

Computer Methods in Applied Mechanics and Engineering, vol. 3, no. 2, pp. 269–289, Mar. 1974, doi: 10.1016/0045-7825(74)90029-2.

[4] "Direct Numerical Simulation - an overview — ScienceDirect Topics." https://www.sciencedirect.com/topics/engineering/direct-numerical-simulation (accessed Mar. 30, 2021).

[5] "Examining Iterative Convergence." https://www.grc.nasa.gov/www/wind/valid/tutorial/iterconv.htm (accessed Apr. 13, 2021).

[6] Fluid Mechanics 101, [CFD] The Courant (CFL) Number. https://www.youtube.com/watch?v=WBWY46ynRk0 2020.

[7] G. Pascarella et al., "COVID-19 diagnosis and management: a comprehensive review," Journal of Internal Medicine, vol. 288, no. 2, pp. 192–206, 2020, doi: 10.1111/joim.13091.

[8] G. Seminara, B. Carli, G. Forni, S. Fuzzi, A. Mazzino, and A. Rinaldo, "Biological fluid dynamics of airborne COVID-19 infection," Rend Lincei Sci Fis Nat, pp. 1–33, Aug. 2020, doi: 10.1007/s12210-020-00938-2.

[9] K. L. Chong, C. S. Ng, N. Hori, R. Yang, R. Verzicco, and D. Lohse, "Extended Lifetime of Respiratory Droplets in a Turbulent Vapor Puff and Its Implications on Airborne Disease

Transmission," Phys. Rev. Lett., vol. 126, no. 3, p. 034502, Jan. 2021, doi: 10.1103/PhysRevLett.126.034502.

[10] K. Zhao, "Effect of Anatomy on Human Nasal Air Flow and Odorant Transport Patterns: Implications for Olfaction," Chemical Senses, vol. 29, no. 5, pp. 365–379, Jun. 2004, doi: 10.1093/chemse/bjh033.

[11] M. E. Rosti, M. Cavaiola, S. Olivieri, A. Seminara, and A. Mazzino, "Turbulence dictates the fate of virus-containing droplets in violent expiratory events," arXiv:2008.05119 [cond-mat, physics:physics], Dec. 2020, Accessed: Jan. 15, 2021. [Online]. Available: http://arxiv.org/abs/2008.05119.

[12] M. Jayaweera, H. Perera, B. Gunawardana, and J. Manatunge, "Transmission of COVID-19 virus by droplets and aerosols: A critical review on the unresolved dichotomy," Environ Res, vol. 188, p. 109819, Sep. 2020, doi: 10.1016/j.envres.2020.109819.

[13] Schriever, Valentin Hummel, Thomas Lundström, Johan Freiherr, Jessica. (2012). Size of nostril opening as a measure of intranasal volume. Physiology behavior. 110-111. 10.1016/j.physbeh.2012.12.007.

[14] W. F. Wells, On air-borne infection: Study II. Droplets and droplet nuclei, Am. J. Epidemiol. 20, 611 (1934).

[15] Zhang, G. Guo, C. Zhu, Z. Ji, and C.-H. Lin, "Transport and trajectory of cough-induced bimodal aerosol in an air-conditioned space," Indoor and Built Environment, p. 1420326X20941166, Jul. 2020, doi: 10.1177/1420326X20941166.

[16] Zhang, G. Guo, C. Zhu, and Z. Ji, "TRANSPORT OF AEROSOL BY COUGHING IN AN AIR-CONDITIONED SPACE," Jan. 2019, pp. 1341–1353, doi: 10.1615/TFEC2019.hbe.028480.

[17] "IV. On the dynamical theory of incompressible viscous fluids and the determination of the criterion," Phil. Trans. R. Soc. Lond. A, vol. 186, pp. 123–164, Dec. 1895, doi: 10.1098/rsta.1895.0004.